Journal of Applied Polymer Science

# Modeling of expandable polystyrene expansion

**Yifeng Hong, Xudong Fang, Donggang Yao**
School of Materials Science and Engineering, Georgia Institute of Technology, Atlanta, Georgia 30332
Correspondence to: X. Fang (E-mail: xfang30@gatech.edu)

**ABSTRACT:** A fundamental understanding of the expansion kinetics of expandable polystyrene (EPS) is crucial for the design and optimization of processes for EPS-filled syntactic foams. In this study, a general formulation was developed to model EPS expansion. A semi-analytical solution was obtained on the basis of the case of a single bubble expansion in an infinite matrix. The dimensionless bubble radius and pressure were defined and found to be exponential functions of the dimensionless expansion time. The characteristic bubble expansion time was able to characterize the timescale of the expansion process. The semi-analytical solution could qualitatively predict the radial expansion of the EPS microsphere observed in a real-time experiment. To obtain an accurate prediction, a numerical solution was obtained to the model that coupled the nucleation and expansion of multiple bubbles in a finite matrix at various temperatures. The results show that the numerical solution was able to quantitatively predict the radial expansion of EPS. A parameter sensitivity study was performed to examine the effect of each parameter over the expansion process. © 2016 Wiley Periodicals, Inc. J. Appl. Polym. Sci. **2016**, *133*, 43886.

**KEYWORDS:** flame retardance; foams; kinetics; polystyrene; theory and modeling

Received 10 December 2015; accepted 3 May 2016
**DOI: 10.1002/app.43886**

## INTRODUCTION

Expandable polystyrene (EPS) is small-diameter polystyrene microsphere containing a physical blowing agent, usually pentane or butane. Solid EPS microspheres can be expanded into foams with closed-cell structures when they are exposed to elevated temperatures. They are the raw materials used to produce polystyrene foams that are widely used in areas such as packaging, construction, automobile, and marine.[1–4] Despite only a few reports, EPS-filled syntactic foam has attracted increasing attention as it has shown a high potential for becoming a novel class of engineering materials. Syntactic foams containing expanded EPS microspheres have a low density with a high strength-to-weight ratio and are effectively toughened to increase crack resistance.[4–6] These appealing features enable them to serve well as lightweight structural materials and floating devices.[7] However, conventional methods for processing EPS-filled syntactic foams usually suffer from difficulties such as poor processability, limited choices of matrix materials, low loading of fillers, and ineffective expansion of EPS.

In a previous study, we designed and developed a microwave expansion process to address these emerging issues in the production of EPS-filled syntactic foams.[8] In this process, unexpanded EPS microspheres were distributed and then directly foamed in an uncured thermosetting matrix with microwave heating. This process design was demonstrated with the capability of effectively expanding highly loaded EPS microspheres. The microwave expansion process was later extended to produce composite polystyrene foams with a unique honeycomb-like structure.[9] The mechanical strength and fire resistance of the composite foams were found to be considerably improved compared with those made of pristine polystyrene. To optimize the microwave expansion process, a further understanding of the fundamental aspect of this process is highly desired. We need to establish a model that can simulate the core part of the process, the expansion of the EPS microsphere, because kinetic parameters related to bubble nucleation and growth cannot be measured easily by experimental methods.

A number of modeling efforts have been made to simulate foaming processes involved with physical blowing agents in polymer melts. The existing methods include but are not limited to the single bubble model,[10–12] cell model,[13–15] influence volume analysis,[16–20] level set method,[21,22] and biphase continuum approach.[23,24] However, these models cannot be directly applied to the EPS expansion process because they almost exclusively focus on foaming processes triggered by a sudden decrease in the system pressure. The expansion of EPS, on the other hand, is started by the heating of the system to the expansion temperature. Moreover, the methods mentioned previously usually only simulate the formation of the cell microstructure but do not take the geometry of the foamed plastics into consideration. However, the geometry of the EPS microsphere must

be considered. This is because the shape and size of the foamed EPS directly impact the morphology and properties of the resulting foam. Another process similar to EPS expansion is the bubble growth of vapor in boiling water. This happens when water is heated to boiling temperature and small air bubbles that are dissolved or adhered to impurities quickly grow and collapse. Existing efforts to model this water boiling process usually have not considered the diffusion of vapor into the expanding bubbles because it plays a minor role.[25,26] However, gas diffusion cannot be neglected in the modeling of EPS microspheres because it is directly related to the nucleation and expansion of bubbles.

In this study, a general formulation was developed to assist in furthering the understanding of the basics of the expansion process of the EPS microsphere. A semi-analytical solution was first obtained to provide a relatively simple tool for understanding and optimizing the expansion process. Dimensionless groups and characteristic parameters were defined. They were then used to analyze the modeling results. To obtain an accurate prediction of EPS expansion, a numerical solution to the model that coupled the nucleation and expansion of multiple bubbles in a finite matrix was subsequently developed. The kinetics and temperature dependence of EPS expansion from the numerical solution were studied and compared with those from the semi-analytical solution. Finally, a parameter sensitivity study was performed to examine the effect of each parameter on the expansion process.

## EXPERIMENTAL

### Materials

Cup-grade unexpanded EPS microspheres (DYLITE F271T, Nova Chemicals Corp., Moon Township, PA) were used in this study. The unexpanded EPS contained approximately 5.6% w/w pentane and had an average diameter of 388.6 ± 17.8 μm.

### Characterization

The rheological properties of polystyrene in EPS were characterized on a controlled-stress rotational rheometer with parallel steel plates 21 mm in diameter (model Thermo Mars II, Thermo Fisher Scientific, Inc., Waltham, MA). The polystyrene was obtained directly from the EPS microspheres used in this study after a vacuum degassing process was performed to remove the pentane inside.

The radial expansion of the EPS microspheres as a function of time was recorded in real time by a hot stage (model T95-HS, Linkam Scientific Instruments, Ltd., United Kingdom) mounted on an Olympus BX51 optical microscope installed with an Olympus UC30 digital camera (Olympus Corp. of the Americas, Center Valley, PA). The hot stage was designed to be placed in a container that could be sealed and whose temperature could be accurately controlled by a temperature controller produced by the hot-stage manufacturer. After the EPS microspheres were put onto the hot stage, the container was closed, and its temperature was quickly raised to the expansion temperature. Images of the EPS microspheres were then taken at very short intervals by the camera. The diameter of each of the EPS microspheres as a function of time was obtained with Olympus Stream Image Analysis Software through the measurement of the axis length across the sphere center. We then calculated the average microsphere radius by halving the number-average diameter.

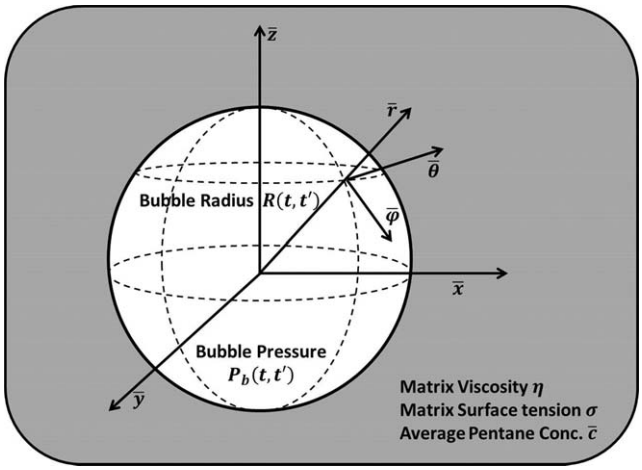


**Figure 1.** Scheme of bubble growth in an EPS matrix.

## MODEL DEVELOPMENT

### General Formulation

Before the expansion, the EPS microspheres were stored at room temperature or at lower temperatures to keep the pentane/polystyrene solution in a stable state. When the microspheres were heated to the expansion temperature, the solution became supersaturated because of a decrease in the pentane solubility. To minimize the free energy of the system, bubble nucleation was begun. The continuous expansion of bubbles was driven by the difference between the bubble pressure ($P_b$) and the ambient pressure ($P_a$). During the expansion of old bubbles, new bubbles were simultaneously nucleated. The termination of the expansion of individual bubbles was reached when $P_b$, $P_a$, and the matrix surface stress are balanced. Because the expansion temperature of EPS is usually lower than that of other plastic foaming processes [this results in a higher matrix viscosity ($\eta$) and a smaller expansion pressure difference], the bubble rupture plays a minor role and, for simplicity, was assumed to be negligible in this study.

A scheme that illustrates the growth of bubbles in the matrix during the EPS expansion process is shown in Figure 1. The bubble radius is defined as $R(t,t')$ and represents the radius at time $t$ of the bubble nucleated at time $t'$ (the bubble nucleation time). The bubble pressure at time $t$ of the bubble nucleated at $t'$ is expressed as $P_b(t,t')$. The average pentane concentration in the EPS matrix at $t'$ is defined as $\bar{c}(t')$. Before expansion, $\bar{c}(t')$ was equal to the initial pentane concentration ($c_0$). The EPS matrix had a surface tension of $\sigma$ and a viscosity of $\eta$. When $t = 0$, the bubble had an initial radius of $R_0$ and an initial bubble pressure of $P_{b0}$.

The bubble was assumed to remain in a spherical shape during the expansion. Then, a spherical coordinate system could be established in each bubble with the coordinate origin fixed at the center of the sphere. The continuity equation of the bubble

with the boundary condition $v_{r|r=R}=\frac{\partial R}{\partial t}$ could be written as follows:

$$v_r = \frac{R^2}{r^2}\frac{\partial R}{\partial t} \tag{1}$$

where $R$ is bubble radius, $r$ is radial distance in the spherical coordinate system in single bubble, and $v_R$ is the bubble expanding velocity in $rr$ direction when $r = R$.

Because the viscosity of the polystyrene matrix was very high during EPS expansion, the effects of gravity and inertia could be neglected.[27] Therefore, the equation of motion in the radial direction is written as follows:

$$0 = -\frac{\partial P}{\partial r} + \frac{\partial \tau_{rr}}{\partial r} + \frac{2(\tau_{rr}-\tau_{\theta\theta})}{r} \tag{2}$$

where $\tau_{rr}$ is the principle stress in $rr$ direction and $\tau_{\theta\theta}$ is the principle stress in $\theta\theta$ direction.

By integrating both sides and substituting the Young–Laplace equation for a spherical bubble and eq. (1) into eq. (2), one can then obtain the following:

$$0 = -\frac{2\sigma}{R} + P_b - P_a + 2\int_R^\infty \frac{(\tau_{rr}-\tau_{\theta\theta})}{r}\,dr \tag{3}$$

Equation (3) is the governing equation that couples the momentum and mass conservations in the bubble expansion.

At the bubble surface, the diffusion of pentane molecules into the bubble can be expressed as follows:

$$\frac{dn_g}{dt} = 4\pi D R^2 \frac{\partial c}{\partial r}\bigg|_{r=R} \tag{4}$$

where $D$ is the diffusion coefficient of pentane in polystyrene, $c$ is the pentane concentration, and $n_g$ is mole number of pentane molecules in the bubble is calculated by the ideal gas law:

$$n_g = \frac{P_b V_b}{\Re T} = \frac{4\pi R^3 P_b}{3\Re T}$$

where $T$ is the temperature of the bubble.

The left hand of eq. (4) represents the changing rate of the molar number of pentane molecules in the bubble and the right hand is the diffusion of pentane from matrix to the bubble.

Therefore, eq. (4) can be reorganized as follows:

$$R\frac{dP_b}{dt} + 3P_b\frac{dR}{dt} = 3D\Re T\frac{\partial c}{\partial r}|_{r=R} \tag{5}$$

Equation (5) is the governing equation that considers the mass balance in the pentane transfer.

In this model, thermal effects are considered to be of negligible importance because the condition of EPS expansion is isothermal.[28] Moreover, because it usually takes only several seconds to fully expand the EPS microspheres, the loss of pentane to the surroundings is not taken into consideration.

**Semi-Analytical Solution**

To obtain a semi-analytical solution to the model developed previously, the bubble is assumed to expand in an infinite EPS matrix of which $\eta$ is constant, and the pentane diffusion through the bubble surface is not considered.

On the basis of these simplifications, eq. (3) can be rewritten as follows:

$$P_b - P_a - \frac{2\sigma}{R} - \frac{4\eta}{R}\frac{\partial R}{\partial t} = 0 \tag{6}$$

Here, several dimensionless groups, including the dimensionless bubble radius ($R^*$), dimensionless bubble pressure ($P_b^*$), and dimensionless expansion time ($t^*$) are defined, namely

$$R^* = \frac{R(P_{b0}-P_a)}{2\sigma} \tag{7}$$

$$P_b^* = \frac{P_b - P_a}{P_{b0}-P_a} \tag{8}$$

$$t^* = \frac{t(P_{b0}-P_a)}{4\eta} \tag{9}$$

With these dimensionless groups, eq. (6) can be rewritten as follows:

$$\frac{dR^*}{dt^*} = P_b^* R^* - 1 \tag{10}$$

The characteristic bubble expansion time ($t_c$) and characteristic bubble radius ($R_c$) are found to be

$$t_c = \frac{4\eta}{P_{b0}-P_a} \tag{11}$$

$$R_c = \frac{2\sigma}{P_{b0}-P_a} \tag{12}$$

According to the ideal gas law, $P_b$ can be correlated with the bubble radius as follows:

$$P_b = \frac{P_{b0}R_0^3}{R^3} \tag{13}$$

The bubble radius can be then numerically solved by the substitution of eq. (13) back to eq. (6). The constants used are given in Table I.[29,30]

To model the expansion process of the EPS microsphere, a bubble nucleation mechanism should have been introduced. However, as pentane diffusion was not considered, existing diffusion-based nucleation theories could not be adopted. Because experiments have shown that nucleation often undergoes an exponential decay, the nucleation rate was assumed to follow an exponential law[31]:

$$J(t') = N_1 \exp\left(-\frac{t'}{N_2}\right) \tag{14}$$

where $J(t')$ is the bubble nucleation rate as a function of $t'$, $N_1$ is a pre-exponential constant ($7.5 \times 10^{14}$ $s^{-1}$ $m^{-3}$), and $N_2$ is a nucleation time constant (0.45 s). The number of bubbles could be calculated through the integration of $J(t')$ from 0 to $t'$. Therefore, the EPS radius $\hat{R}(t)$ can be calculated by the following expression:

$$\hat{R}(t') = \sqrt[3]{\hat{R}_0^3 + V_0\int_0^{t'} J(t')R^3(t,t')\,dt} \tag{15}$$

where $\hat{R}_0$ is the initial radius of the EPS microsphere and $V_0$ is the initial volume of the EPS microsphere.

**Table I.** Summary of the Constants and Characteristic Parameters in the Semi-Analytical Solution

| Expansion temperature | $\eta$ ($\times 10^5$ Pa s) | $\sigma$ (N/m) | $P_{b0}$ ($\times 10^5$ Pa) | $t_c$ (s) | $R_c$ ($\times 10^{-8}$ m) |
|---|---|---|---|---|---|
| 130 °C | 3.02 | 0.034 | 11.04 | 1.200 | 6.53 |
| 140 °C | 1.33 | 0.033 | 13.31 | 0.43 | 5.21 |
| 150 °C | 0.61 | 0.032 | 15.92 | 0.16 | 4.20 |

**Numerical Solution**

In the aforementioned study, the model was simplified to obtain a semi-analytical solution based on a single bubble growth in an infinite matrix. It has been found that the semi-analytical solution can only qualitatively predict the radial expansion of EPS. Detailed results are shown in the Results and Discussion section. To more accurately predict the expansion of EPS, we developed a numerical solution on the basis of the nucleation and expansion of multiple bubbles in a finite matrix at various temperatures considering the diffusion of pentane.

A classical heterogeneous nucleation theory was applied to describe the bubble nucleation process of EPS expansion.[32] The nucleation rate was modeled as follows:

$$J(t') = f_0 \bar{c} \sqrt{\frac{2\sigma N_A^3}{\pi M_w}} \exp\left(-\frac{\Delta E F}{k_B T}\right) \tag{16}$$

where $f_0$ is the Zeldovich correction factor, $N_A$ is Avogadro's number, $M_w$ is the molecular weight of pentane, $F$ is the free-energy barrier correction factor, $\Delta E$ is the free energy barrier,

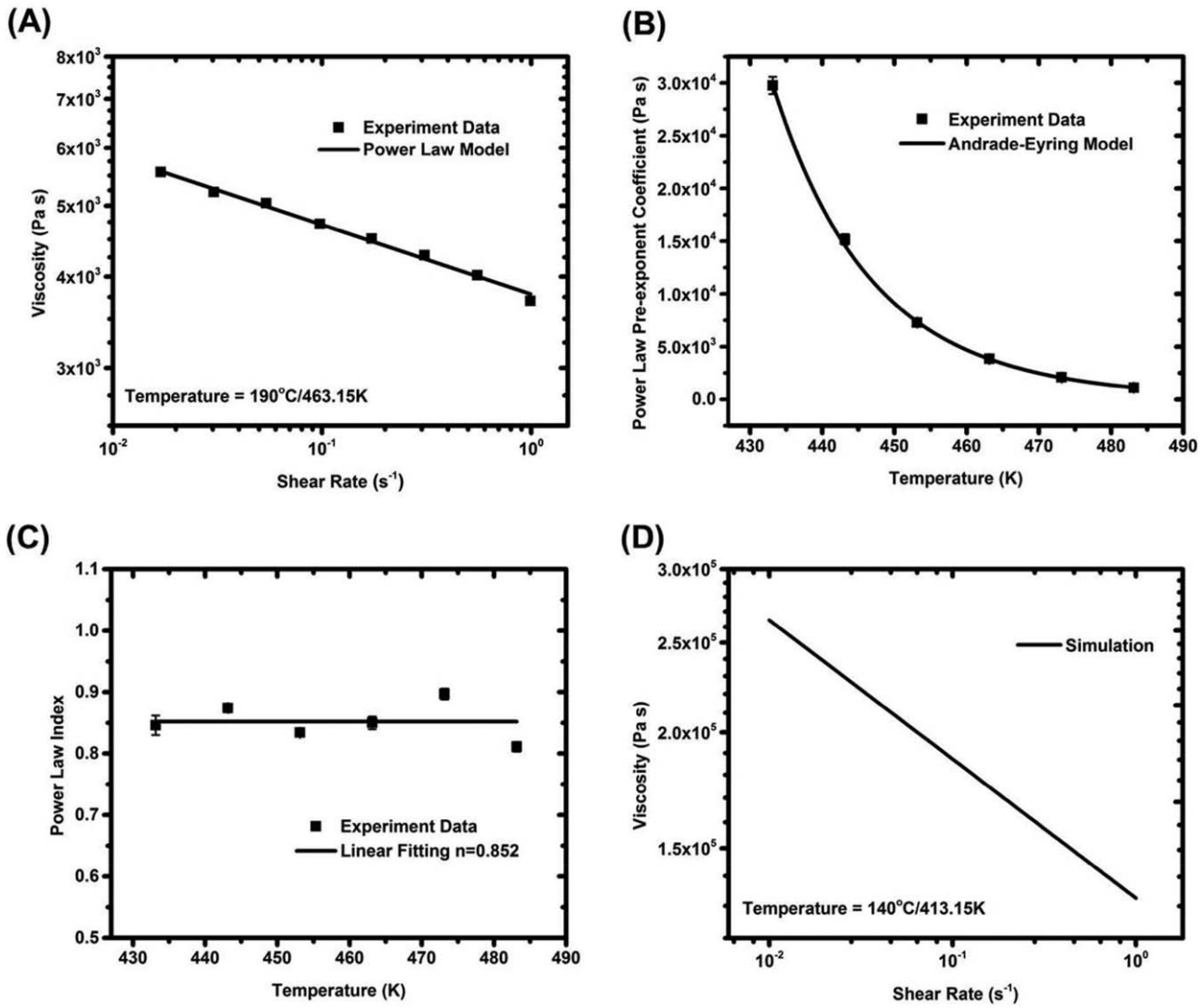


**Figure 2.** (A) Power law model fit to polystyrene viscosity as a function of the shear rate at 190 °C. (B) Andrade–Eyring model fit to the power law model $\eta_0$ as a function of the temperature. (C) Linear fit to the power law model index as a function of the temperature. (D) Predicted polystyrene viscosity as a function of the shear rate at 140 °C.

**Table II.** Summary of the Constants in the Numerical Solution

| | Symbol | Value | Units |
|---|---|---|---|
| Ambient pressure | $P_a$ | $1.01 \times 10^5$ | Pa |
| Critical saturated pressure of pentane | $P_{b0}c$ | $3.37 \times 10^6$ | Pa |
| Critical temperature | $T^c$ | 469.7 | K |
| Generalized Wagner equation constants | $c_1$ | −7.349492 | — |
| | $c_{1.5}$ | 2.382017 | — |
| | $c_2$ | −2.176618 | — |
| | $c_3$ | 0.891296 | — |
| | $c_4$ | −3.841503 | — |
| Zeldovich correction factor | $f_0$ | $3.15 \times 10^{-22}$ | — |
| Free-energy barrier correction factor | $F$ | $6.74 \times 10^{-5}$ | — |
| Power law model index | $n$ | 0.852 | — |
| Andrade–Eyring model pre-exponent constant | $K$ | $5.11 \times 10^{-10}$ | Pa/s |
| Andrade–Eyring model activation energy | $E_\eta$ | $1.14 \times 10^5$ | J/mol |
| Diffusion coefficient pre-exponent constant | $D_0$ | $2.42 \times 10^{11}$ | $m^2/s$ |
| Diffusion activation energy | $E_D$ | $1.59 \times 10^5$ | J/mol |
| Initial pentane concentration | $c_0$ | $7.04 \times 10^2$ | $mol/m^3$ |
| Diffusion radius correlation constant | β | 1.842 | — |
| Henry's solubility constant | $k_H$ | $7.8 \times 10^{-9}$ | Pa $mol^{-1}$ $m^{-3}$ |

and $k_B$ is Boltzmann's constant. The number of bubbles can be calculated through the integration of $J(t')$ from 0 to $t'$.

$\Delta E$ is expressed as follows:

$$\Delta E = \frac{16\pi\sigma^3}{3(P_{b0}-P_a)^2} \tag{17}$$

where σ can be expressed by the following semi-empirical equation[33]:

$$\sigma = \left[4.07\times10^{-2}-7.2\times10^{-5}(T-293)\right]\cdot N\cdot m^{-1} \tag{18}$$

The temperature dependence of the saturated pentane pressure ($P_{b0}$) was calculated with the generalized Wagner model[30]:

$$\ln P_{b0} = \ln P_{b0}^c + \frac{T^c}{T}\left(c_1\tau + c_{1.5}\tau^{1.5} + c_2\tau^2 + c_3\tau^3 + c_4\tau^4\right) \tag{19}$$

where $P_{b0}{}^c$ is the critical saturated pressure of pentane, $T^c$ is the critical temperature, and τ is a reduced temperature that can be expressed as follows:

$$\tau = 1 - \frac{T}{T^c} \tag{20}$$

Because the pentane only occupied approximately a 5.6% weight fraction in EPS, it was reasonable to assume that the rheological behavior of the polystyrene represented that of the pentane/polystyrene solution. As shown in Figure 2(A), the viscosity of polystyrene as a function of the shear rate could be fitted well by a power law model[34]:

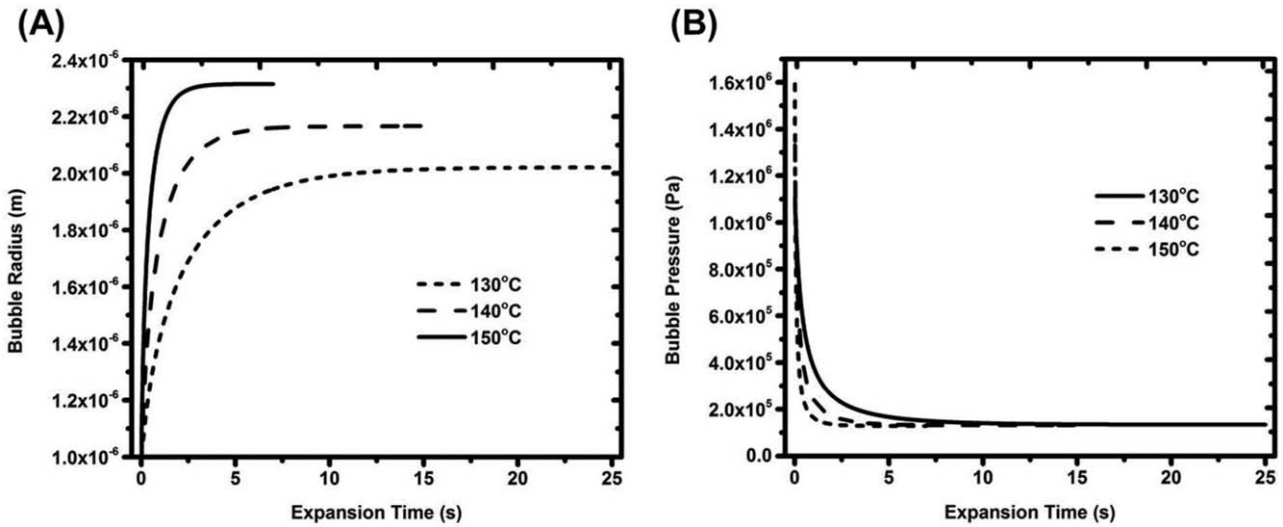


**Figure 3.** (A) Bubble radius and (B) $P_b$ as a function of the expansion bubble time in the semi-analytical solution.

**Table III.** Summary of the Constants in the Exponential Fitting of $R^*$ and $P_b^*$ as Functions of $t^*$ in the Semi-Analytical Solution

| Expansion temperature | $A_{A1}$ | $A_{A2}$ | $A_{A3}$ |
|---|---|---|---|
| 130 °C | 14.03 ± 0.025 | 1.95 ± 0.006 | 30.77 ± 0.006 |
| 140 °C | 19.93 ± 0.048 | 2.44 ± 0.009 | 41.48 ± 0.008 |
| 150 °C | 27.78 ± 0.110 | 2.92 ± 0.018 | 54.91 ± 0.017 |
| Expansion temperature | $B_{A1}$ | $B_{A2}$ | $B_{A3}$ |
| 130 °C | 0.81 ± 0.006 | 0.78 ± 0.008 | 0.031 ± 0.0005 |
| 140 °C | | | |
| 150 °C | | | |

$$\underline{\underline{\tau}} = \eta_0 \sqrt{\frac{1}{2}|\underline{\underline{\dot{\gamma}}} : \underline{\underline{\dot{\gamma}}}|^{n-1}}\,\underline{\underline{\dot{\gamma}}} \tag{21}$$

where $n$ is the power law index and $\eta_0$ is the pre-exponent coefficient, $\underline{\underline{\tau}}$ is shear stress tensor and $\underline{\underline{\dot{\gamma}}}$ is the shear rate tensor. With eq. (1), the second invariant in the power law model can be written as follows:

$$\frac{1}{2}\underline{\underline{\dot{\gamma}}} : \underline{\underline{\dot{\gamma}}} = 12\left(\frac{R^2}{r^3}\frac{\partial R}{\partial t}\right)^2$$

A detailed derivation process of eq. (21) is shown in Ref. 35.

Then, through the substitution of eq. (21) into eq. (3), the following equation can be obtained:

$$P_b - P_a - \frac{2\sigma}{R} - \frac{4\eta_0}{n}\left(2\sqrt{3}\right)^{n-1}\left(R^2\frac{\partial R}{\partial t}\right)^n \frac{1}{R^{3n}} = 0 \tag{22}$$

As shown in Figure 2(B), the temperature dependence of $\eta_0$ can be approximated with the Andrade–Eyring model[27]:

$$\eta_0 = K\exp\left(\frac{E_\eta}{\Re T}\right) \tag{23}$$

where $K$ is the Andrade–Eyring model pre-exponent constant, $E_\eta$ is the Andrade–Eyring model activation energy, and $\Re$ is the universal gas constant. $n$ at different temperatures was found to be approximately 0.852 [Figure 2(C)]. Therefore, the temperature dependence of the rheological behavior of polystyrene was obtained. The predicted polystyrene viscosity as a function of the shear rate at 140 °C is shown in Figure 2(D).

When we assumed that pentane followed Henry's law,[36] the gas concentration profile at the surface of a bubble could be expressed as follows:

$$\frac{\partial c}{\partial r}|_{r=R} = \frac{1}{\beta R}(\bar{c} - k_H P_b) \tag{24}$$

where $k_H$ is Henry's solubility constant and $\beta$ is the diffusion radius correlation constant.

The average pentane concentration ($\bar{c}$) was calculated by the following equation:

$$\frac{d\bar{c}}{dt} = -\frac{4\pi D}{\beta}\int_0^{t'} J(t')R(\bar{c} - P_b k_H)dt' \tag{25}$$

The temperature dependence of the diffusion coefficient ($D$) was found to follow an Arrhenius equation[37]:

$$D = D_0\exp\left(-\frac{E_D}{\Re T}\right) \tag{26}$$

where $D_0$ is the diffusion coefficient pre-exponent constant and $E_D$ is the diffusion activation energy.

We numerically solved the accurate model by coupling the governing equations developed previously. The constants in the model are summarized in Table II.[29,30,36,37]

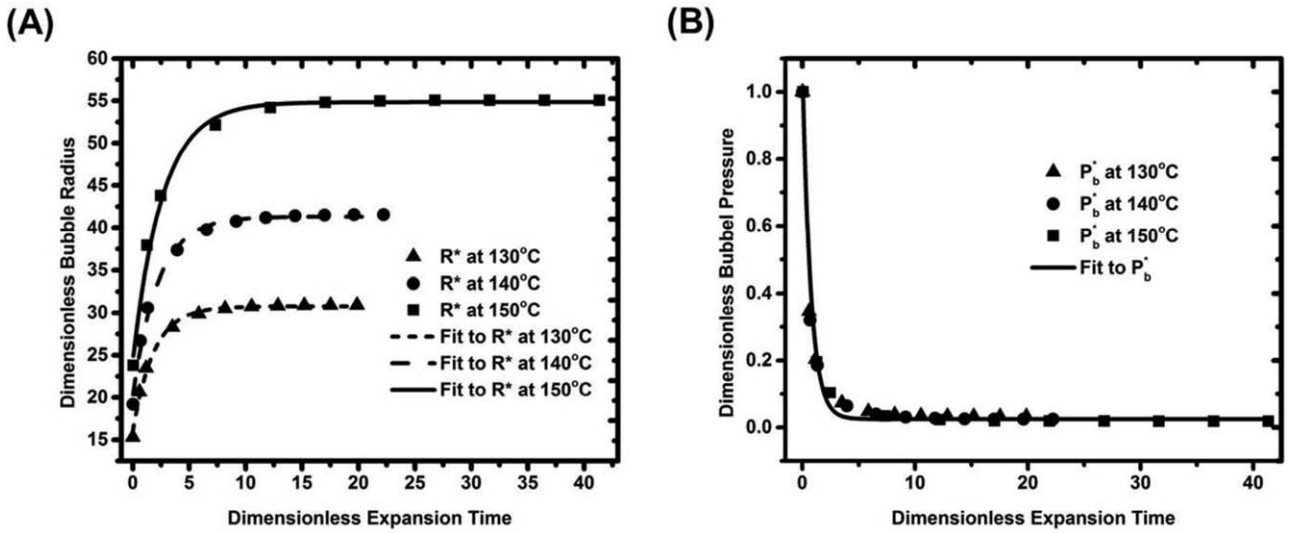


**Figure 4.** (A) $R^*$ and (B) $P_b^*$ as a function of $t^*$ in the semi-analytical solution.

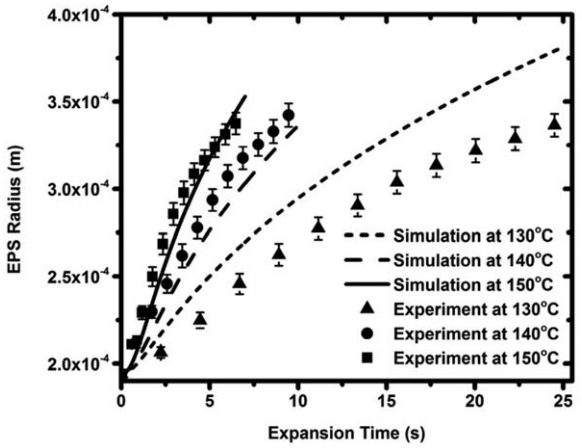


**Figure 5.** Comparison of the experimental radial growth of EPS and the predicted growth from the semi-analytical solution at different temperatures.

## RESULTS AND DISCUSSION

### Semi-Analytical Solution

The results of bubble radius growth as a function of time are presented in Figure 3(A). Generally, the radius of the bubble increased very fast after the start of expansion until an equilibrium state was reached when $P_b$ was equal to the sum of $P_a$ and the surface stress. Similar trends were also found in the change of $P_b$, as presented in Figure 3(B). $P_b$ dropped very quickly to the equilibrium state during the expansion of bubbles.

$t_c$ is an important characteristic parameter; it is correlated with the properties of both the matrix and the bubble. It can be used to characterize the timescale of the expansion of bubbles. As shown in Table I, $t_c$ decreased with increasing expansion temperature. This was because a higher expansion temperature resulted in a lower $\eta$ and larger $P_{b0}$. Therefore, we further deduced that the rates of bubble radius growth and $P_b$ dropped at higher temperature would be larger. This deduction was confirmed by the results shown in Figure 3. Another important

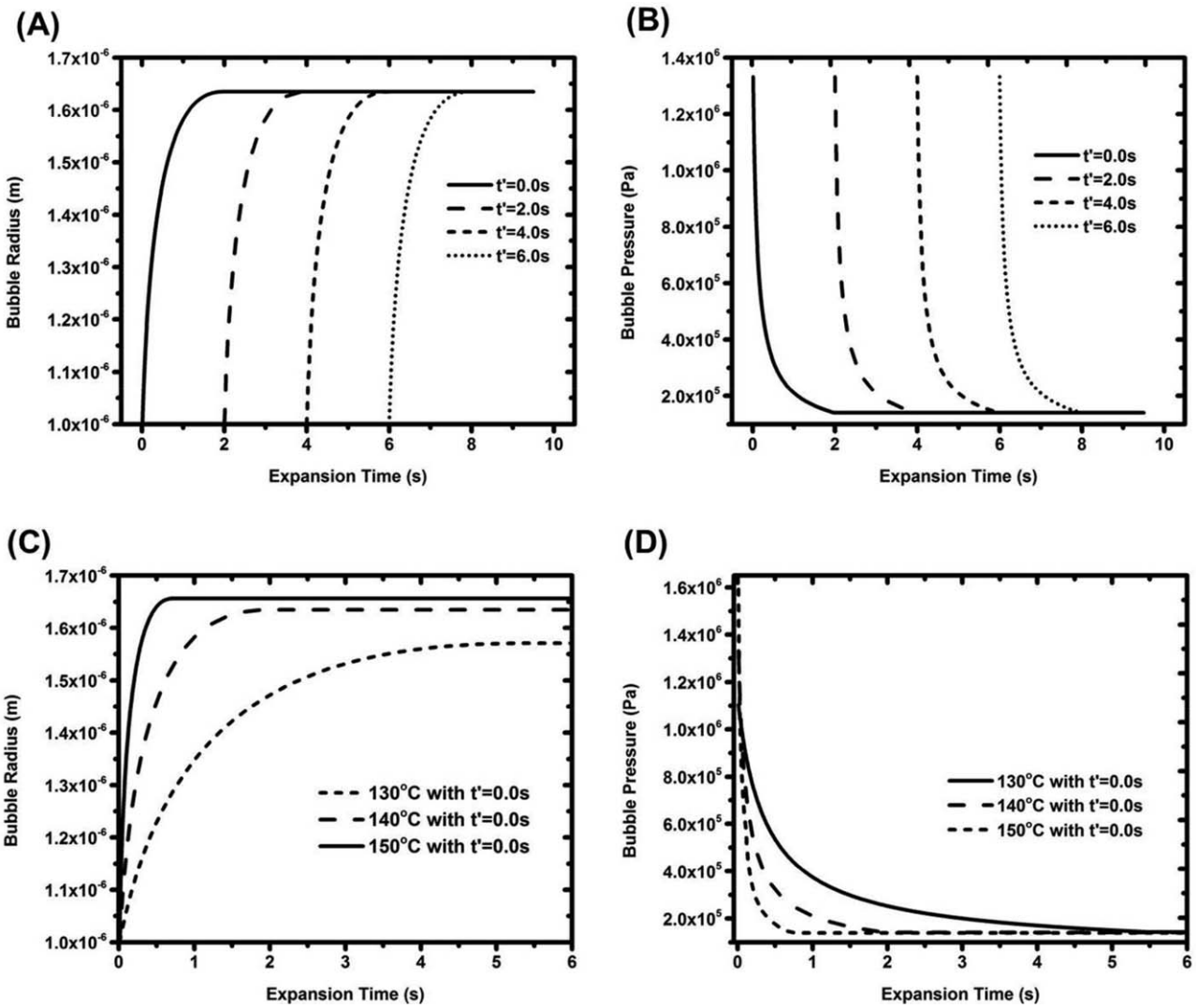


**Figure 6.** (A) Bubble radius as a function of the expansion time and nucleation time at 140 °C, (B) $P_b$ as a function of the expansion time and nucleation rate at 140 °C, (C) bubble radius (with nucleation at 0.0 s) as a function of the expansion time at various temperatures, and (D) $P_b$ (with nucleation at 0.0 s) as a function of the expansion time at various temperatures in the numerical solution.

**Table IV.** Summary of the Constants in the Exponential Fitting of $R^*$ and $P_b^*$ as Functions of $t^*$ in the Numerical Solution

| Expansion temperature | $A^{N1}$ | $A_{N2}$ | $A_{N3}$ |
|---|---|---|---|
| 130 °C | 8.77 ± 0.047 | 0.90 ± 0.001 | 24.06 ± 0.009 |
| 140 °C | 12.43 ± 0.075 | 0.88 ± 0.002 | 31.38 ± 0.013 |
| 150 °C | 16.83 ± 0.031 | 0.84 ± 0.004 | 39.44 ± 0.005 |
| Expansion temperature | $B_{N1}$ | $B_{N2}$ | $B_{N3}$ |
| 130 °C | 1.01 ± 0.022 | 0.51 ± 0.029 | 0.037 ± 0.0067 |
| 140 °C | | | |
| 150 °C | | | |

characteristic parameter was $R_c$; we could use this to characterize the size of the equilibrated bubble radius. We correlated this with the bubble surface energy and pressure difference. The former applied the resistance to the expanding bubbles, whereas the latter was the driving force for the expansion. As presented in Table III and Figure 3(A), with increasing $R_c$, the ultimate bubble radius increased.

With the obtained bubble radius and pressure, $R^*$ and $P_b^*$ could be calculated with eqs. (7) and (8), respectively. We found that in a large range of temperatures, $R^*$ and $P_b^*$ were functions of $t^*$, according to the following exponential relations:

$$R^* = -A_{A1}\exp\left(-\frac{t^*}{A_{A2}}\right)+A_{A3} \quad (27)$$

$$P_b^* = B_{A1}\exp\left(-\frac{t^*}{B_{A2}}\right)+B_{A3} \quad (28)$$

where $A_{Ai}$ and $B_{Ai}$ ($i = 1$, 2, and 3) are constants that are dependent on the expansion temperature. Their values are summarized in Table III. We observed that whereas the values of $A_{Ai}$ changed at different expansion temperatures, $B_{Ai}$ remained the same; this indicated that $R^*$ was more sensitive to the variation of temperature.

The fitting results are presented in Figure 4. We observed that the growth rate of $R^*$ increased with increasing $t_c$ and reached a larger ultimate value, which corresponded to a smaller $t_c$ and a larger $R_c$. The temperature, however, had little influence over $P_b^*$. As the simple exponential relation of $R^*$ and $P_b^*$ can be applied in a large range of expansion temperatures, the expansion kinetics of the bubbles could thus be easily estimated, and this could assist in the design of the process.

The radial expansion of the whole EPS microsphere could be calculated with an exponential bubble nucleation expression. The comparison between the experimental and modeling results is shown in Figure 5. We observed that the semi-analytical solution was able to predict, at least at a qualitative level, the radius growth of the expanding EPS microspheres obtained from a real-time observation at different expansion temperatures. Moreover, a faster expansion was obtained when $t_c$ was smaller. However, we also found that the prediction curve had a relatively larger deviation from the experimental results at a lower temperature. This was because the semi-analytical model did not consider the diffusion of pentane from the matrix into the bubble. The diffusion was temperature dependent. When the temperature was low, the diffusivity of pentane was lower. That could explain why the semi-analytical model overpredicted the growth of EPS microspheres at 130 °C.

This simple semi-analytical solution could be used to easily analyze the expansion kinetics of the bubbles and EPS

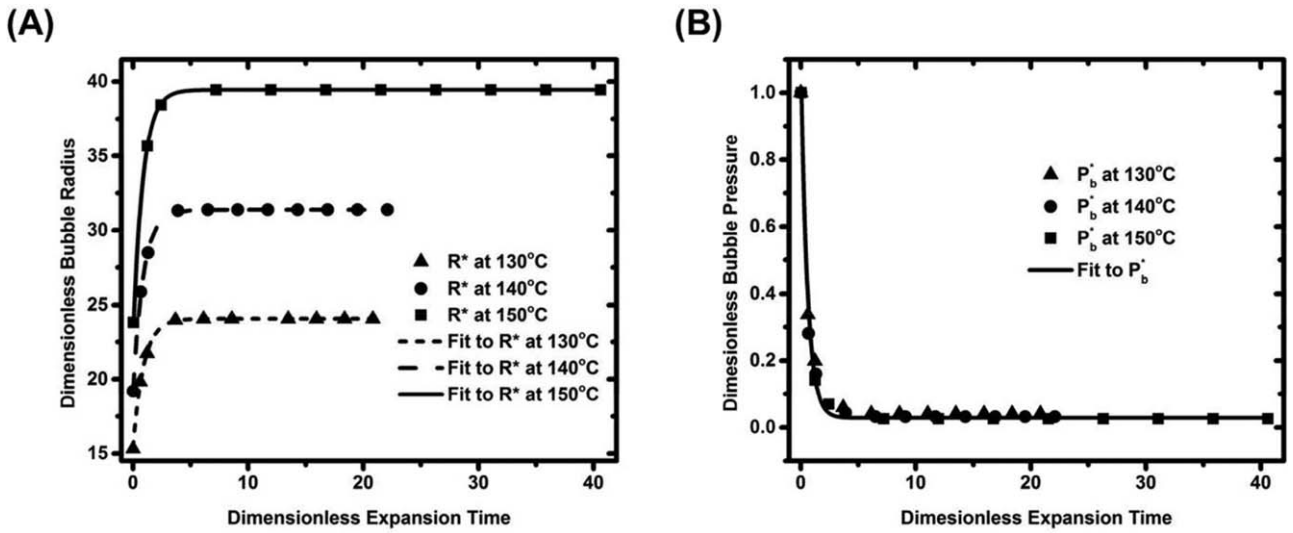


**Figure 7.** (A) $R^*$ and (B) $P_b^*$ as a function of $t^*$ in the numerical solution.

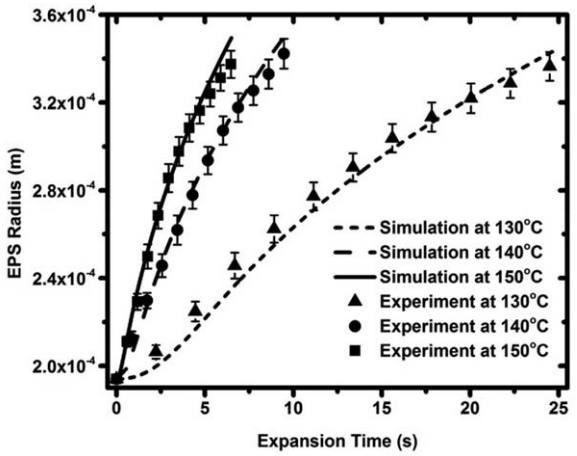


**Figure 8.** Comparison of the experimental radial growth of EPS and the predicted growth from the numerical solution at different temperatures.

microspheres; this provided references to the design and optimization of the expansion process. However, such a solution can only lead to a qualitative prediction for the actual expansion process because several nonrealistic simplifications were involved in the solution development. First, the bubble expansion was assumed to take place in an infinite matrix. However, the matrix is usually finite in actual cases. Second, the pentane transfer was assumed to be neglected between the bubble and the matrix. This was not true because, during the bubble expansion, the pentane dissolved in polystyrene diffused into the bubble because of the existence of a concentration gradient. For the same reason, the existing bubble nucleation theory could not be correlated with the semi-analytical solution. Third, the viscosity of the EPS matrix was assumed to be constant, but it is widely acknowledged that the polystyrene viscosity is shear-rate dependent. Therefore, to obtain a quantitative prediction of the actual expansion process of the EPS microspheres, the model without these simplifications needed to be solved.

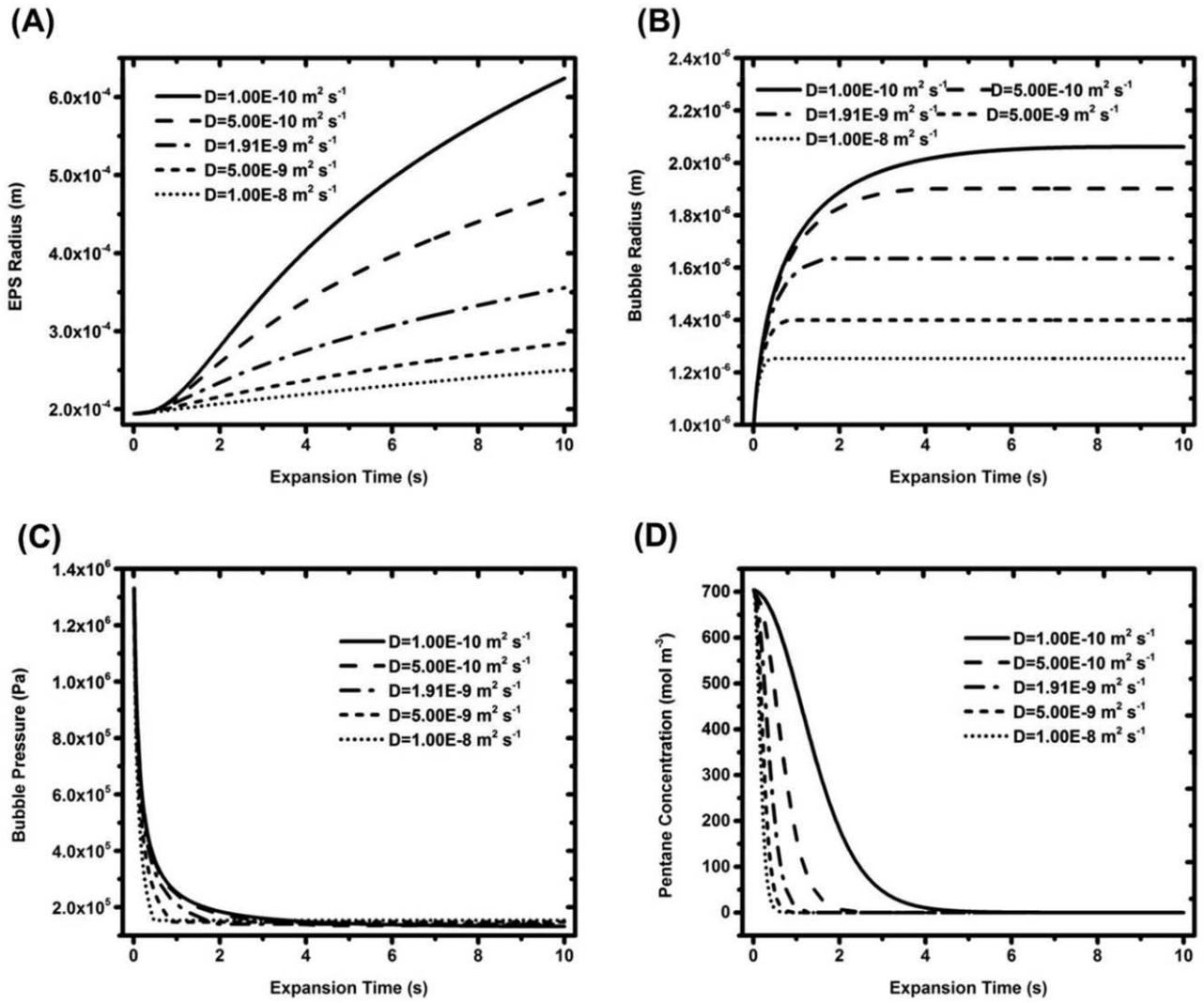


**Figure 9.** Sensitivity study of the influence of the diffusion coefficient on the (A) EPS radius, (B) bubble radius, (C) $P_b$, and (D) $\bar{c}$ in a pentane/polystyrene solution in the numerical model (expansion temperature = 140 °C).

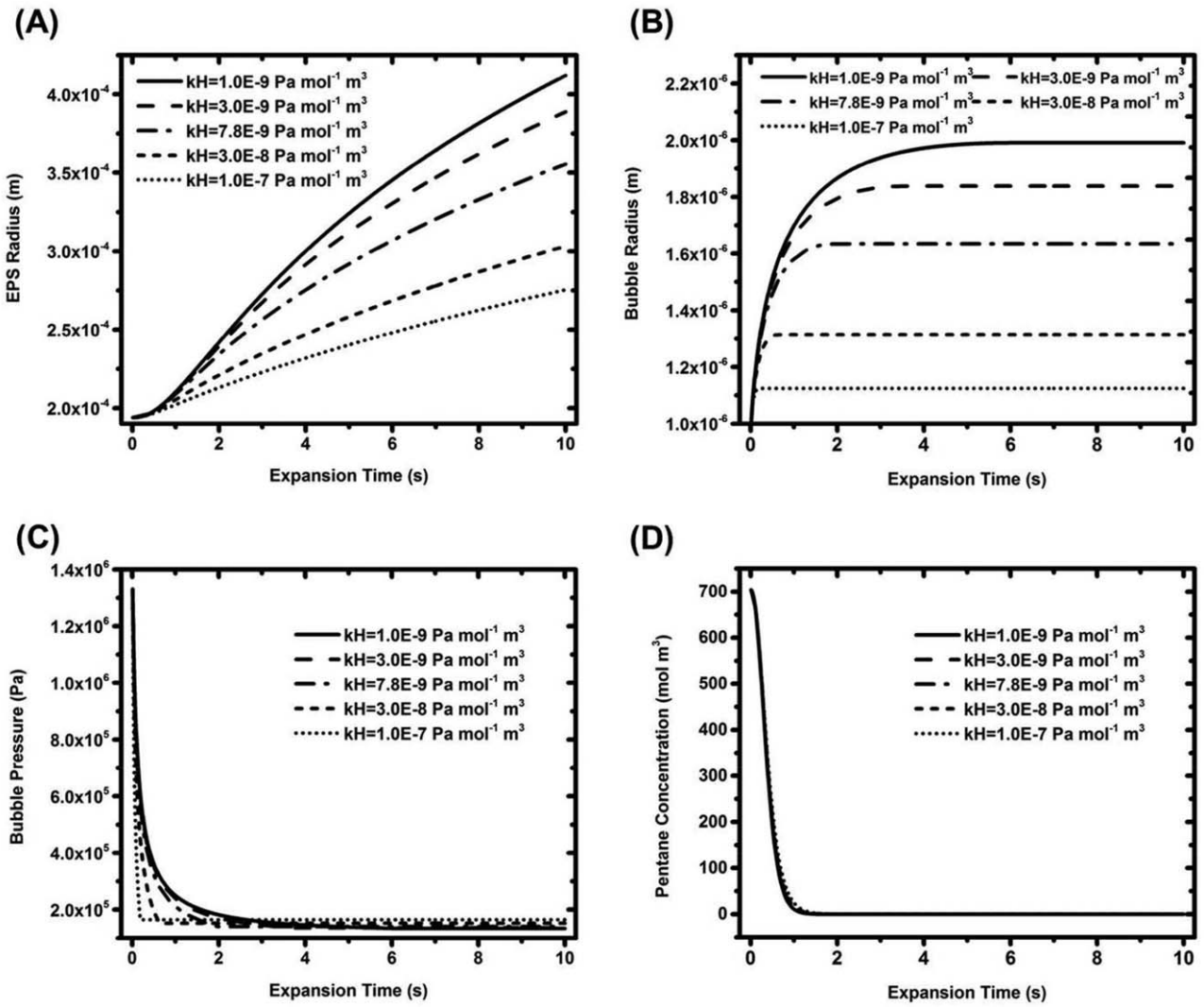


**Figure 10.** Sensitivity study of the influence of Henry's law constant on the (A) EPS radius, (B) bubble radius, (C) $P_b$, and (D) $\bar{c}$ in a pentane/polystyrene solution in the numerical model (expansion temperature = 140 °C).

### Numerical Solution

To obtain the quantitative prediction of EPS expansion, a numerical solution that coupled the nucleation and expansion of multiple bubbles in a finite matrix at various expansion temperatures was developed under the general formulation. The diffusion of pentane and the rate dependence of EPS η were taken into consideration.

The expansion kinetics of the bubble is presented in Figure 6. As shown in Figure 6(A,B), the bubble radius grew very fast in the initial several seconds after nucleation. Meanwhile, $P_b^*$ dropped quickly. The rates of the radius increase and pressure decrease gradually slowed down to zero when the bubble expansion reached an equilibrium state. Bubbles nucleated at different times followed a very similar expansion pattern. The radius growth of bubbles that were nucleated at 0.0 s as a function of the expansion temperature is shown in Figure 6(C). A higher growth rate of the bubble radius was reached when a higher expansion temperature was used; this corresponded to a smaller $t_c$. We also noticed that with increasing expansion temperature, the equilibrated bubble radius also increased in accordance with the reverse changing trend of $R_c$. Figure 6(D) represents the dropping rate of $P_b$ as a function of the expansion temperature. As shown in eq. (19), $P_{b0}$ increased with increasing expansion temperature. The pressure dropping rate of the bubbles nucleated at 0.0 s was also found to increase as the temperature rose. The equilibrated $P_b$s at different expansion temperatures were very similar. This was because, compared with σ, $P_a$ played a more influential role in determining the balanced $P_b$.

Similar to the semi-analytical solution, $R^*$ and $P_b^*$ were also found to be as functions of $t^*$ according to the exponential relations

$$R^* = -A_{N1}\exp\left(-\frac{t^*}{A_{N2}}\right)+A_{N3} \tag{29}$$

$$P_b^* = B_{N1}\exp\left(-\frac{t^*}{B_{N2}}\right)+B_{N3} \tag{30}$$

where $A_{Ni}$ and $B_{Ni}$ ($i = 1, 2, 3$) are constants that are dependent on the expansion temperature. Their values are summarized in

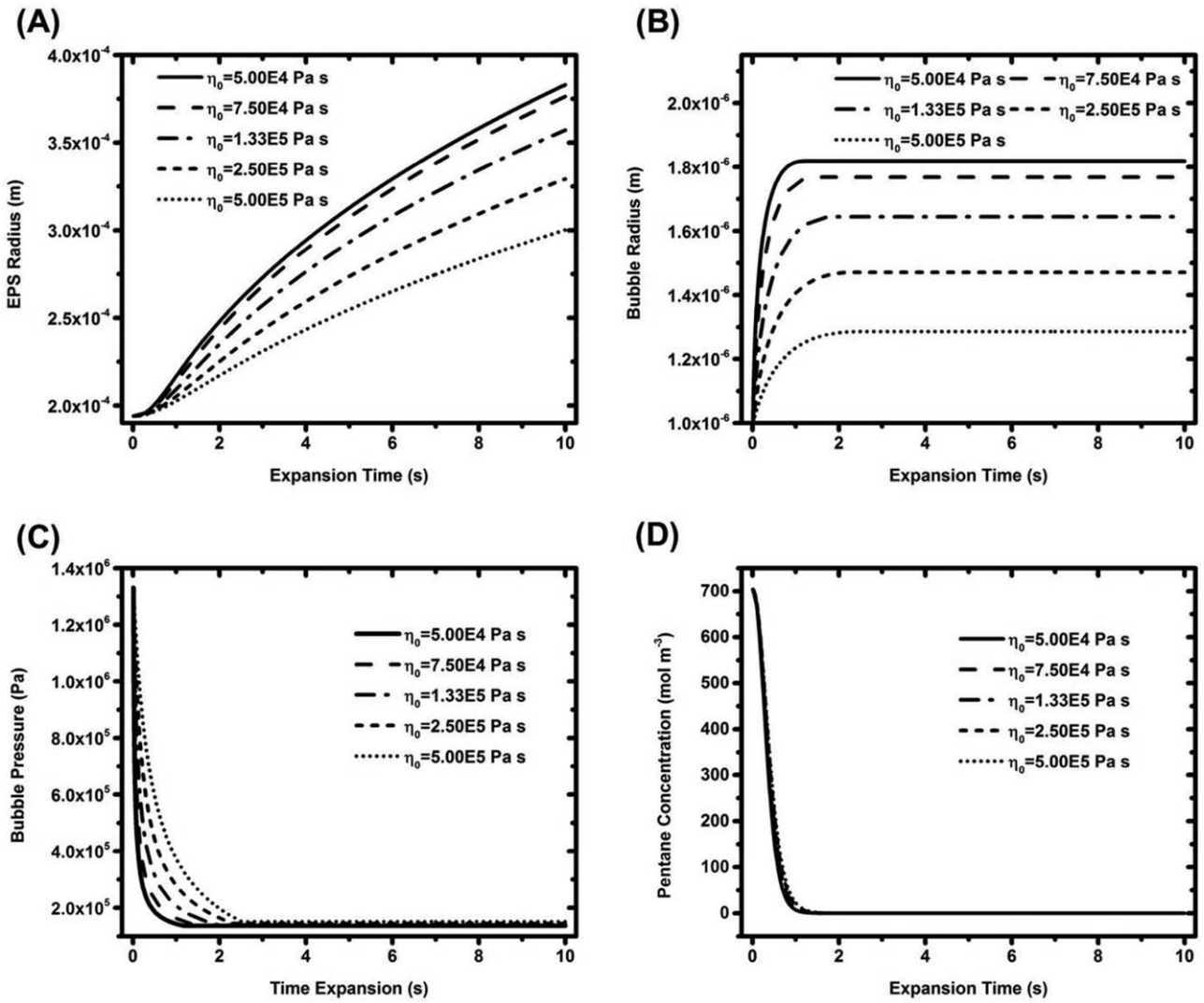


**Figure 11.** Sensitivity study of the influence of the power law pre-exponent constant on the (A) EPS radius, (B) bubble radius, (C) $P_b$, and (D) $\bar{c}$ in a pentane/polystyrene solution in the numerical model (expansion temperature = 140 °C).

Table IV. As $B_{Ni}$ remained the same in a large range of temperatures, we deduced that $P_b^*$ was less sensitive to the variation of temperature. Moreover, the $A_{Ni}$ were smaller than $A_{Ai}$ at the same temperature of expansion; this corresponded to a slower growth rate of $R^*$ and a smaller equilibrated dimensionless radius. The comparison between $B_{Ni}$ and $B_{Ai}$ led to a similar result. This was because, in contrast with semi-analytical solution, the numerical solution modeled the expansion of the bubble in a finite matrix with the consideration of the pentane diffusion process.

The results of the dimensionless analysis on the numerical solution are also summarized in Figure 7. As shown in Figure 7(A), we observed that a higher expansion temperature, corresponding to a shorter $t_c$ and a smaller $R_c$, led to a larger growth rate and equilibrated size of $R^*$. As indicated in Table IV and shown in Figure 7(B), the variation of the expansion temperature had limited influence over $P_b^*$, which could be fitted by an exponential function with $t^*$ as an independent variable in a large range of temperatures.

Figure 8 compares the experimental results of the radial expansion of EPS with the predicted ones at various temperatures. In contrast with the semi-analytical solution, the numerical solution could more quantitatively predict the experimental results obtained from the real-time observation at each of the selected temperatures. We observed that with increasing expansion temperature, the growth rate of the EPS radius increased; this corresponded to a smaller $t_c$.

Furthermore, by comparing the prediction results between the semi-analytical model and the numerical model, we found that the overprediction at low temperature, which existed in the semi-analytical model, did not happen in the solution of numerical model. This was because in the numerical model, we considered the diffusion of pentane from the matrix to the bubble during the development of the formula. Not only did this influence the bubble expansion process, as the gas diffusion was one of the major driving forces in expansion, but this also affected the bubble nucleation kinetics, whose rate was lowered with the decrease of the pentane dissolved in the polystyrene. Another difference between the two

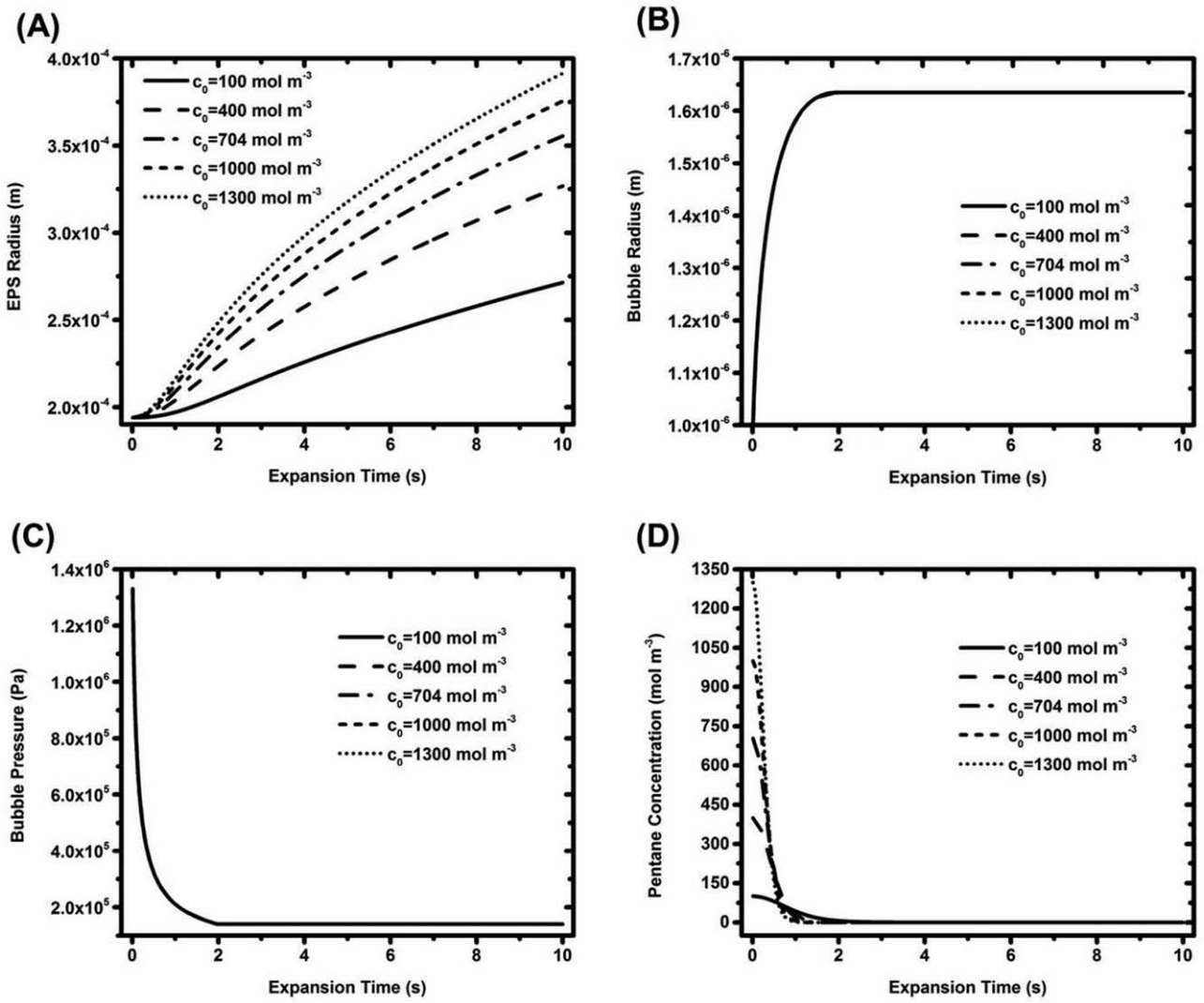


**Figure 12.** Sensitivity study of the influence of $c_0$ on the (A) EPS radius, (B) bubble radius, (C) $P_b$, and (D) $\bar{c}$ in a pentane/polystyrene solution in the numerical model (expansion temperature = 140 °C).

models was that the numerical model considered both the temperature and shear effects over the viscosity of the matrix, whereas only the temperature influence was involved in the semi-analytical model. This enabled the numerical model to more accurately simulate the growth of the bubbles. The semi-analytical model, which required fewer parameters, was designed to provide users with a simple tool to qualitatively and quickly examine the expansion kinetics of EPS. This simplicity enabled the semi-analytical model to be incorporated into a more complicated large-scale process model, which only required reasonable accuracy. The numerical model, on the other hand, was designed to provide a more accurate prediction and a tool that assists in the study of expansion kinetics and the design of the EPS system. More details are provided in the Parameter Sensitivity Study section.

### Parameter Sensitivity Study

In the numerical solution, many parameters simultaneously influenced the modeling results. It was worth performing a sensitivity study on them; we included study of the diffusion coefficient, Henry's law constant, power law pre-exponent constant, and $c_0$. This was because with such a study, we could evaluate the effect of each parameter to assist in the design and optimization of the expansion system. In the parameter sensitivity study, whereas a set of conditions with the variation of a single parameter was in the run. The others remain unchanged.

The results of the sensitivity study on the influence of the diffusion coefficient over the expansion kinetics of the EPS microspheres at 140 °C are summarized in Figure 9. As presented in Figure 9(A), a higher growth rate of the EPS radius was found to be with a lower diffusion coefficient. This was because the bubble radius could reach a larger equilibrium value with decreasing diffusion coefficient, as shown in Figure 9(B). As shown in Figure 9(C), we found that the dropping rate of $P_b$ was lowered at a smaller diffusion coefficient because the diffusion of pentane from the EPS matrix into the bubble slowed down. For a similar reason, the variation of $\bar{c}$ in the pentane/polystyrene matrix also slowed down, as shown in Figure 9(D).

The influence of the variation of Henry's law constant was very similar to that of the diffusion coefficient. As shown in Figure 10(A), with increasing Henry's law constant, we observed that the radius of the EPS microspheres grew faster because the ultimate radius of the bubble was increased, as shown in Figure 10(B). A lower Henry's law constant was also able to slow down the diffusion of pentane from the EPS matrix to the bubbles, as presented in Figure 10(C). However, it seemed that the change in Henry's law constant had a relatively limited influence over $\bar{c}$ in the pentane/polystyrene solution, as shown in Figure 10(D).

The results of the sensitivity study on the influence of the power law pre-exponent constant over the expansion kinetics of the EPS microspheres are shown in Figure 11. As shown in Figure 11(A), we found that the radius growth rate of the EPS microsphere increased as the power law pre-exponent constant was lowered because there was less resistance to the expansion of bubbles. This was confirmed by the results of the bubble radius growth, shown in Figure 11(B). Moreover, as the bubble growth rate increased at a lower viscosity, the dropping rate of $P_b$ also increased, as shown in Figure 11(C). A shown in Figure 11(D), $\bar{c}$ in the EPS matrix seemed to be less affected by the variation of $\eta$.

The initial concentration of pentane in the EPS microspheres was found to have a significant influence over the expansion kinetics of the EPS microspheres. As shown in Figure 12(A), because $J(t')$ increased when $c_0$ increased, we found that the EPS radius grew faster at a higher initial concentration of pentane. However, because $c_0$ did not influence the parameters that controlled the diffusion of the gas, it had very limited influence over the increase of the bubble radius and the decrease of $P_b$, as presented in Figure 12(B,C), respectively. Similarly, as shown in Figure 12(D), we found that $c_0$ did not have much influence over $\bar{c}$ in the matrix of the EPS microspheres.

## CONCLUSIONS

In this study, a general formulation was developed to model the expansion process of the EPS microspheres. A semi-analytical solution was first obtained on the basis of the simplified case of a single bubble expansion in an infinite matrix. This solution provides a relatively simple tool for understanding and optimizing the expansion process. $R^*$ and $P_b^*$ were obtained as exponential functions of $t^*$. $t_c$ was able to characterize the timescale of the expansion process. The equilibrated bubble radius was in reverse proportion to $R_c$. The semi-analytical solution could qualitatively predict the experimental results of the radial expansion of the EPS microspheres obtained in a real-time observation. However, this solution suffered from some unrealistic simplifications, including an infinite matrix, the exclusion of pentane diffusion, and the constant viscosity of polystyrene.

To obtain a more accurate prediction of EPS expansion, a numerical solution was then developed to the model that was correlated with the nucleation and expansion of multiple bubbles in a finite matrix at various expansion temperatures. The diffusion process of pentane and the rate-dependent viscosity of the EPS matrix were considered. We discovered that the numerical solution was able to quantitatively predict the expansion of EPS microspheres. The temperature also played an important role in determining the expansion kinetics. With increasing the expansion temperature, the process could be considerately accelerated. Finally, a parameter sensitivity study was performed to examine the effect of each parameter on the expansion process. We found that the growth rate of EPS microspheres during expansion could be increased with decreases in the diffusion coefficient, Henry's law constant, and $\eta$ or increases in the initial concentration of pentane.

## ACKNOWLEDGMENTS

The authors acknowledge Nova Chemicals Corp. for generously providing unexpanded F271T EPS microspheres and Meisha Shofner at the Georgia Institute of Technology for the use of the Linkam hot stage.

## REFERENCES

1. Tomalino, M.; Bianchini, G. *Prog. Org. Coat.* **1997**, *32*, 17.
2. Bharadwaj-Somaskandan, S.; Krishnamurthi, B.; Sergeeva, T.; Shutov, F. *J. Elastomers Plast.* **2003**, *35*, 325.
3. Kim, N. H.; Kim, H. S. *J. Appl. Polym. Sci.* **2005**, *98*, 1663.
4. Aglan, H.; Shebl, S.; Morsy, M.; Calhoun, M.; Harding, H.; Ahmad, M. *Constr. Build. Mater.* **2009**, *23*, 2856.
5. Kim, H. S.; Kim, N. H. *J. Appl. Polym. Sci.* **2006**, *100*, 4045.
6. Lawrence, E.; Pyrz, R. *Polym. Polym. Compos.* **2001**, *9*, 227.
7. Klempner, D.; Sendijarevic, V. Polymeric Foams and Foam Technology, 2nd ed.; Hanser Gardner: Cincinnati, OH, **2004**.
8. Hong, Y.; Fang, X.; Yao, D. *Polym. Eng. Sci.* **2015**, *55*, 1818.
9. Hong, Y.; Fang, X.; Yao, D. *Polym. Eng. Sci.* **2015**, *55*, 1494.
10. Epstein, P. S.; Plesset, M. S. *J. Chem. Phys.* **1950**, *18*, 1505.
11. Scriven, L. E. *Chem. Eng. Sci.* **1959**, *10*, 1.
12. Barlow, E. J.; Langlois, W. E. *IBM J. Res. Dev.* **1962**, *6*, 329.
13. Amon, M.; Denson, C. D. *Polym. Eng. Sci.* **1984**, *24*, 1026.
14. Arefmanesh, A.; Advani, S. G.; Michaelides, E. E. *Int. J. Heat Mass Transfer* **1992**, *35*, 1711.
15. Arefmanesh, A.; Advani, S. C. *Polym. Eng. Sci.* **1995**, *35*, 252.
16. Joshi, K.; Lee, J. G.; Shafi, M. A.; Flumerfelt, R. W. *J. Appl. Polym. Sci.* **1988**, *67*, 1353.
17. Otsuki, Y.; Kanai, T. *Polym. Eng. Sci.* **2005**, *45*, 1277.
18. Leung, S. N.; Park, C. B.; Li, H. *Plast. Rubber Compos.* **2006**, *35*, 93.
19. Leung, S. N.; Park, C. B.; Xu, D. L.; Li, H. B.; Fenton, R. G. *Ind. Eng. Chem. Res.* **2006**, *45*, 7823.
20. Al-Moameri, H.; Zhao, Y. S.; Ghoreishi, R.; Suppes, G. J. *Ind. Eng. Chem. Res.* **2016**, *55*, 2336.
21. Rao, R. R.; Mondy, L. A.; Noble, D. R.; Moffat, H. K.; Adolf, D. B.; Notz, P. K. *Int. J. Numer. Methods Fluids* **2012**, *68*, 1362.
22. Seo, D.; Youn, J. R. *Polymer* **2005**, *46*, 6482.

23. Markert, B. *Arch. Comput. Methods Eng.* **2008**, *15*, 371.
24. Thorat, R.; Bruining, H. *Transport Porous Media* **2016**, *112*, 53.
25. Chang, D. L.; Lee, C. F. F. *Proc. Combust. Inst.* **2005**, *30*, 2737.
26. Mukherjee, A.; Kandlikar, S. G. *Microfluidics Nanofluidics* **2005**, *1*, 137.
27. Macosko, C. W. Rheology: Principles, Measurements, and Applications; Wiley-VCH: New York, **1994**.
28. Joshi, K.; Lee, J. G.; Shafi, M. A.; Flumerfelt, R. W. *J. Appl. Polym. Sci.* **1998**, *67*, 1353.
29. Tuladhar, T. R.; Mackley, M. R. *Chem. Eng. Sci.* **2004**, *59*, 5997.
30. Ewing, M. B.; Ochoa, J. C. S. *J. Chem. Thermodyn.* **2006**, *38*, 289.
31. Lauri, A. Theoretical and Computational Approaches on Heterogeneous Nucleation; University of Helsinki: Helsinki, **2006**.
32. Liao, R. G.; Yu, W.; Zhou, C. X. *Polymer* **2010**, *51*, 568.
33. Park, C. B.; Suh, N. P. *Polym. Eng. Sci.* **1996**, *36*, 34.
34. Larson, R. G. The Structure and Rheology of Complex Fluids; Oxford University Press: New York, **1998**.
35. Favelukis, M.; Albalak, R. J. *Chem. Eng. J.* **1996**, *63*, 149.
36. Mao, D. M.; Edwards, J. R.; Harvey, A. *Chem. Eng. Sci.* **2006**, *61*, 1836.
37. Fike, L. R. Transport Properties of Polystyrene above and below Glass Transition Temperature; Texas Tech University: Lubbock, TX, **1983**.